Eddahbi, M., Muñoz, A., Savoini, B. & Monge, M. (2019). Mechanical properties and microstructure of W/CuY and W/CuCrZr composites produced by hot isostatic pressing. *Fusion Engineering and Design*, vol. 146, pp. 1829–1833.

DOI: 10.1016/j.fusengdes.2019.03.045

Mechanical properties and microstructure of W/CuY and W/CuCrZr composites produced by hot isostatic pressing

M. Eddahbi[1], A. Muñoz[1,2*], B. Savoini[1,2], M.A. Monge[1,2]

[1]*Universidad Carlos III de Madrid, Dpto. de Física, Avda. de la Universidad 30, Leganés 28911-Spain*
[2]*Instituto Tecnológico de Química y Materiales Álvaro Alonso Barba (IAAB), Avda. de la Universidad 30, Leganés 28911-Spain*

Fully dense W-15wt%CuY and W-15wt%CuCrZr composites have been produced by a powder metallurgy route and hot isostatic pressing. The consolidate materials show homogeneous distributions of pre-alloyed CuY and CuCrZr embedded in W phase. Y-enriched particles were found inside the CuY phase. Their mechanical behavior was studied under uniaxial compression from room temperature to 500 ºC. W/CuY exhibited a higher value of the yield strength, but W/CuCrZr presented a larger compressive deformation. Both composites manifested strain hardening during plastic deformation. The deformed microstructure at 250 ºC and 500 ºC was characterized by electron backscatter diffraction (EBSD) measurements and nanoindentation. The correlation between the plastic deformation, grain size and misorientation distributions, has been revealed.

Keywords: tungsten, copper, composite, yttrium, plastic deformation, EBSD.

1. Introduction

Tungsten-copper (W/Cu) composites appear to be promising materials for the divertor cooling system of the future fusion reactors [1]. W/Cu composites combine the high electrical and thermal conductivity and high ductility of copper, with refractoriness and high erosion resistance of tungsten. This combination of properties allows these composites to be used in other different fields [2,3].

The joining of tungsten to copper-based heat sink systems continue being a demanding task for the development of plasma facing components, since the coefficient of thermal expansion is very different in both materials [4]. The presence of a W/Cu composite between both materials could facilitate the joining. Numerous processing routes, such as liquid phase sintering, high torsion, hydrogen reduction, hot isostatic pressing (HIP), mechanical alloying, extrusion, and infiltration, have been attempted to produce fully dense W/Cu materials with a Cu content ranging from 10 to 50 wt% [5,6]. However, it is difficult to achieve a full-densified W/Cu composite, as W and Cu are mutually insoluble [7,8]. Special attention must be paid to the plastic characteristics and hot deformation behavior of these materials, and to establish the correlation between composition, microstructure and plastic behavior.

The present paper reports the microstructure and the mechanical properties under compression from room temperature (RT) up to 500 ºC of W-15wt%CuY and W-15wt%CuCrZr composites produced by HIP. Also, the plastic deformation has been correlated with the grain orientation determined by electron backscattered diffraction measurements (EBSD). The content of CuY and CuCrZr was chosen to optimize the correlation between the mechanical and thermal properties at moderate temperatures of the composites [5].

2. Experimental procedure

W-15wt%CuY and W-15wt%CuCrZr, named as W/CuY and W/CuCrZr, were produced by a powder metallurgy route. The initial raw powders were W, CuY and CuCrZr, with nominal compositions Cu-0.8wt%Y and Cu-0.7wt%Cr-0.1wt%Zr. The powder size distributions, obtained by the laser light scattering technique, are shown in Fig. 1, and the resulting mean powder particle sizes for W, CuY and CuCrZr are 5, 25 and 35 μm, respectively. For each composite, the powders were mixed during 6 h in a Tubular mixer under a high purity Ar atmosphere to produce a homogenous powder dispersion. Subsequently, the blended powders were canned, degassed in vacuum at 300 ºC for 24 h and consolidated by HIP at 925 ºC for W/CuY and at 1050 ºC for W/CuCrZr under a pressure of 180 MPa for 2 h. The density of the composites after consolidation was determined by a He ultra-pycnometer, with resulting values of ~98.1 and ~98.8 % of the theoretical density for W/CuY and W/CuCrZr, respectively. A LECO© analyzer was used for determining the oxygen content. The obtained value for W/CuY diminished from 0.081% for the degassed powder to 0.039% after HIP consolidation and from 0.043 to 0.022% for W/CuCrZr.

The microstructure of the sintered composites was studied by scanning electron microscopy (SEM) with a PHILIPS XL-30 microscope equipped with an energy-dispersive spectroscopy system. The compressive tests were performed on Ø 6 mm × 8 mm cylindrical samples from RT up to 500 °C at a strain rate of 10^{-4} s^{-1}. The nanohardness measurements were carried out at RT in a IMicro nanoindenter, applying a maximum load of 25

author's email: angel.munoz@uc3m.es

mN at a constant strain rate of 0.2% s^{-1}. The distance between indents was 15 μm.

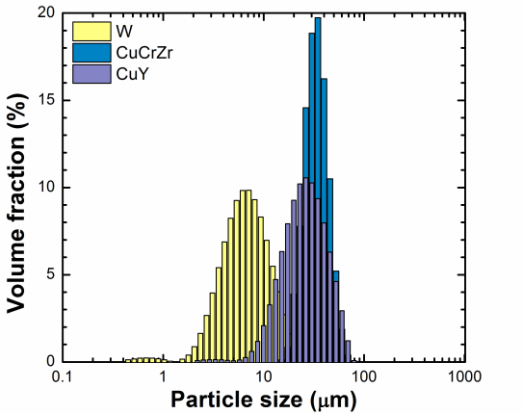

Fig. 1. Powder particle size distribution of the initial raw powders.

The misorientation angle between grains and the grain size distributions were determined from EBSD measurements recorded with a FEG JEOL JSM-6500F microscope. The analysis of the results was performed using the MATLAB MTEX software for quantitative texture analysis [9]. The grain boundaries exhibiting misorientation below 15º were considered as Low Angle Grain Boundaries (LAGBs) and those above 15º as High Angle Grain Boundaries (HAGBs).

3. Results and Discussion

3.1 Microstructure after HIP

The microstructure of the W/CuY and W/CuCrZr after sintering by HIP is presented in Fig. 2. In the SEM micrographs, two phases can clearly be distinguished: the tungsten (light contrast) and the copper-based compound (dark grey contrast), the latter forming large pools homogeneously distributed. The shape and size of the original W powder particles are maintained, as it can be appreciated in the insets images of Fig. 2. It is noted that, although many W particles are linked together, most of them are joined by the copper-based phases. For the W/CuY composite, yttrium-enriched precipitates are observed inside the CuY pools. The presence of cavities or pores is not observed in both composites, in good agreement with the densification measurements.

3.2 Mechanical properties

Fig. 3 depicts the plastic true stress-true strain curves of the uniaxial compression test to failure for the composites in the range from RT to 500 ºC. Both materials exhibit strain hardening, which is more pronounced for W/CuY than for W/CuCrZr, but diminishes on increasing the temperature. Conversely, W/CuCrZr presents larger compressive deformation. This is due to the greater ductility of the CuCrZr, in comparison with CuY. It is noted that the maximum compressive strain in both materials is attained at 250 ºC. The mechanical response of the composites to uniaxial compression is influenced by thermal residual stresses developed during the cooling step of the production process and the heating during the compression tests, resulting from the mismatch in the thermal expansion coefficient of the components.

A nanohardness mapping of the surface of both composites after HIP is presented in Figs. 4a and 4b. The mapping allows to distinguish the two phases present in W/CuY and W/CuCrZr. The areas with the smaller nanohardness values correspond to CuY or CuCrZr, whereas the zones with the higher values correspond to the W particles.

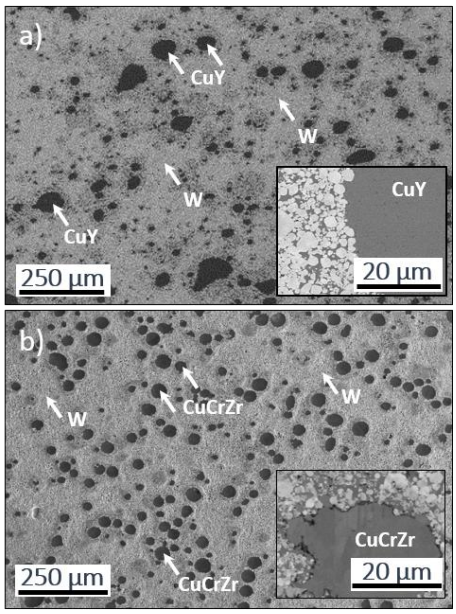

Fig. 2. SEM images of the composites. (a) W/CuY, (b) W/CuCrZr. The insets images correspond to a high magnification of neighborhood of the copper-based particles: (a) CuY and (b) CuCrZr particle.

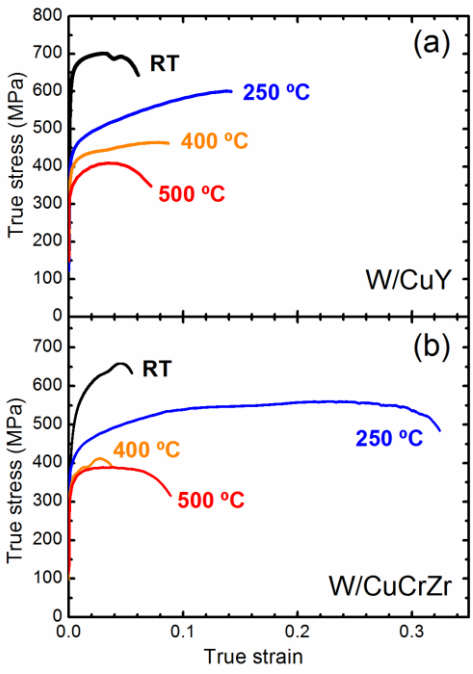

Fig. 3. Compressive true stress-true strain curves at a strain rate of 10^{-4} s^{-1}. (a) W/CuY; (b) W/CuCrZr.

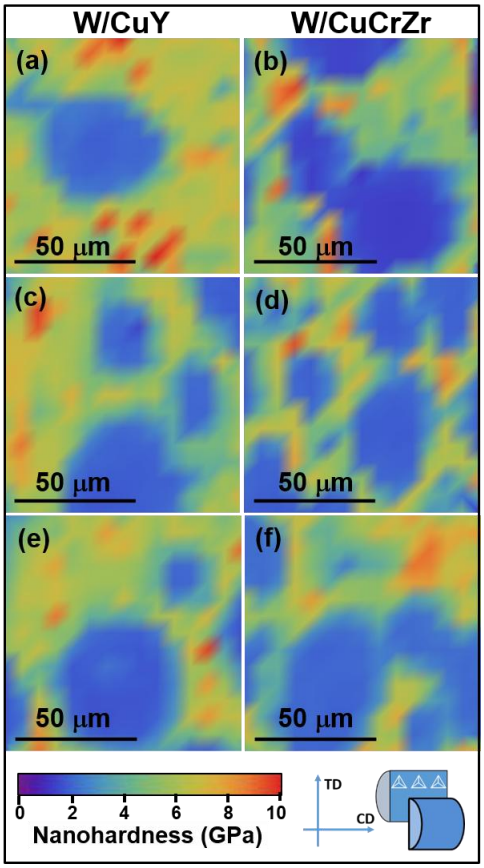

Fig. 4. Nanoindentation mapping at RT of W/CuY and W/CuCrZr. After HIP: (a) and (b); after the compression tests at: 250 ºC (c) and (d), and 500 ºC (e) and (f).

The zones with intermediate nanohardness values do not correspond to a phase formed by copper-based compounds dissolved in tungsten, since W and Cu are nearly insoluble. These areas are formed by small particles of tungsten surrounded by CuY or CuCrZr. As the indent size is big enough for testing both W and Cu-based compounds particles, these zones show an average nanohardness value.

3.3 Characterization after compression tests

3.3.1 Nanohardness mapping

The nanohardness mapping of the composite surfaces after the compression tests are shown in Figs. 4c-f. The measurements have been performed in planes parallel to the compression axis. As it has already been mentioned, the nanohardness values allow distinguishing between the copper-based compounds particles and the tungsten ones. It is observed that the CuY and CuCrZr regions are deformed after compression tests. However, this effect is not observed in the W particles, which indicates the stress reached during the compression tests is not high enough to originate plastic deformation of the W particles. The deformation of CuY/CuCrZr islands controls the strain of the composites, greatly improving the ductility of the composite compared with pure tungsten.

3.3.2 EBSD measurements

Fig. 5 corresponds to images obtained from EBSD measurements of the composites after to failure compression testing, being the horizontal axis of the images parallel to the compression direction. The grain size (Fig. 6) and misorientation distributions (Fig. 7) were determined. For comparison, the results corresponding to the as-HIP condition have also been included.

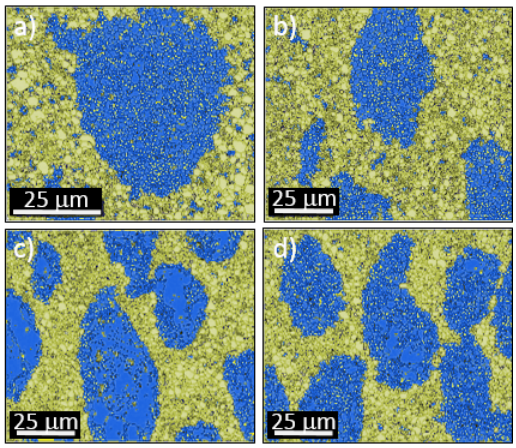

Fig. 5. Microstructure after compression obtained from the EBSD measurements. W/CuY: at 250 ºC (a) and at 500 ºC (b); W/CuCrZr: at 250 ºC (c) and at 500 ºC (d). The blue particles correspond to the copper-based phases whereas the yellow particles correspond to tungsten.

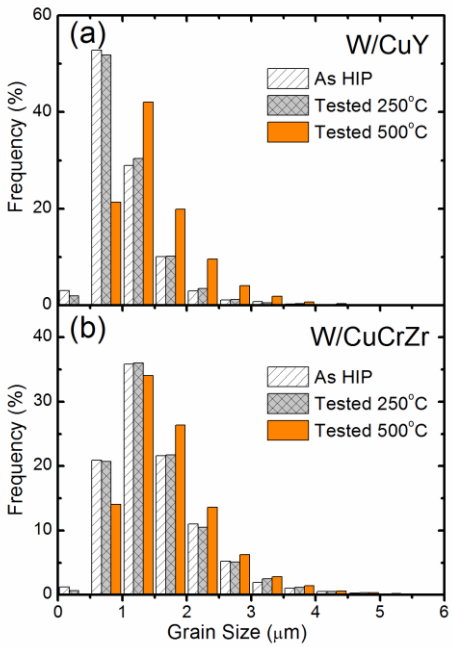

Fig. 6. Grain size distributions obtained from EBSD measurements W/CuY (a) and W/CuCrZr (b).

As observed in Fig. 5, the copper-based particles are clearly embedded in the tungsten matrix, with the CuCrZr pools more elongated than the CuY ones after compression. The grain size distributions of W/CuY show a slight change after hot compression tests, in comparison with the as-HIP condition, while W/CuCrZr hardly changes (see Figs. 6a and 6b). For W/CuY composite the average grain sizes are ~1.1 and ~1.5 μm at 250 ºC and 500 ºC, respectively, whereas for

W/CuCrZr the average grain size is ~1.6 μm for both temperatures. As the temperature of the compression tests is very low compare with the recrystallization temperature of tungsten, the observed changes in the grain size should be attributed to the recrystallization of the copper-based phases.

The grain boundaries misorientation distributions in both composites for as-HIP state and after compression test at 200 and 500 ºC are represented in Fig. 7. As shown in the inset histograms of Figs. 7a and 7b, the W/W misorientations distributions remain unchanged after the compression test, and the corresponding distributions fit a Mackenzie random distribution. That suggests that the compression stress was not high enough to induce changes in the W/W boundaries. For the CuY phase the grain boundaries misorientation distribution in as-HIP state exhibits a bimodal distribution of LAGBs and HAGBs. However, the frequency of LAGBs increases after hot compression test. The CuCrZr exhibits a similar behavior, with LAGBs prevailing over HAGBs after compression tests (see Fig. 7b). These results indicate that the deformation mechanism in both composites should be controlled by extended dynamic recovery (or dynamic continuous recrystallization) in the copper-base compounds.

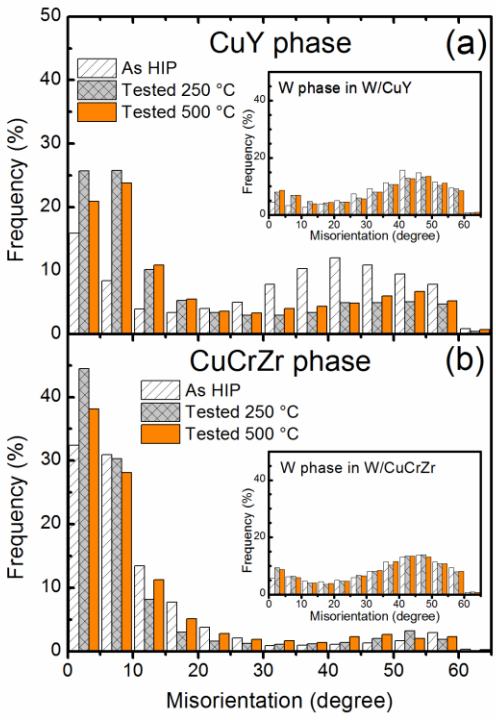

Fig. 7. Misorientation distributions obtained from EBSD measurements. W/CuY (a) and W/CuCrZr (b). The inset histograms correspond to the misorientations in the W phase.

4 Conclusions

Full dense W-15CuY and W-15CuCrZr composites were produced by mechanical alloying and HIP. The CuY and CuCrZr phases were distributed forming pools in the W phase and in the interstices among W powder particles. W-15CuY exhibited a higher yield strength. Strain hardening was observed in the compressive true stress-true strain curves of both composites, which decreased with increasing the temperature. EBSD measurements of the composites deformed at 250 ºC and 500 ºC show that compressive stress originates the appearance of microtexture associated to the deformation of the copper-based phases. The change of the grain sizes and misorientaions distributions in both composites indicate that the hot compressive behavior should be controlled by continuous dynamic recrystallization in the copper compounds.

Future works will be addressed to the thermal behavior and the mechanism governing the hot compressive deformation of these composites. Also, new composites with different CuY and CuCrZr contents will be explored.

Acknowledgments

The present work has been supported by the Ministerio de Economía y Competitividad of Spain (ENE2015-70300-C3-2-R MINECO/FEDER) and the Regional Government of Madrid through TECHNOFUSIÓN(III)CM (P2018/EMT-4437) and MULTIMAT-CHALLENGE (S2013/MIT-2862) programs.

References

[1] E. Autissier et al., Elaboration and thermomechanical characterization of W/Cu functionally graded materials produced by Spark Plasma Sintering for plasma facing components, Fusion Engineering and Design 98-99 (2015) 1929-1932.

[2] J.L. Johnson et al., The Effects of Composition and Microstructure on the Thermal Conductivity of Liquid-Phase-Sintered W-Cu, Metallurgical and Material Transactions A, 41A (2010) 1564-1572.

[3] L.L. Dong et al., Recent progress in development of tungsten-copper composites: Fabrication, modification and applications, Int. J. Refract. Met. Hard Mater. 75 (2018) 30-42.

[4] Jeong-Ha You, Copper matrix composites as heat sink materials for water-cooled divertor target, Nuclear Materials and Energy 5 (2015) 7-18.

[5] A. V. Müller et al., Melt infiltrated tungsten-copper composites as advanced heat sink materials for plasma facing components of future nuclear fusion devices, Fusion Engineering Design 124 (2017) 455-459.

[6] Dongguo Lin, et al., High temperature compression behavior of W-10wt.%Cu composite, Int. J. Refract. Met. Hard Mater. 53 (2015) 87-91.

[7] T.B. Massalski, Binary Alloy Phase Diagrams, 2nd ed., vol. 2. Ohio: ASM; 1990.

[8] J. Song, et al., Preparation of W–Cu functionally graded material coated with CVD–W for plasma-facing components, Journal of Nuclear Materials, 442 (2013) S208-S213.

[9] R. Hielscher and H. Schaeben, A novel pole figure inversion method: specification of the MTEX algorithm, Journal of Applied Crystallography, 41 (2008) 1024-1037.

[10] J. Crank, The Mathematics of Diffusion, Clarendon Press, Oxford, 1975.

Figure 1
Click here to download high resolution image

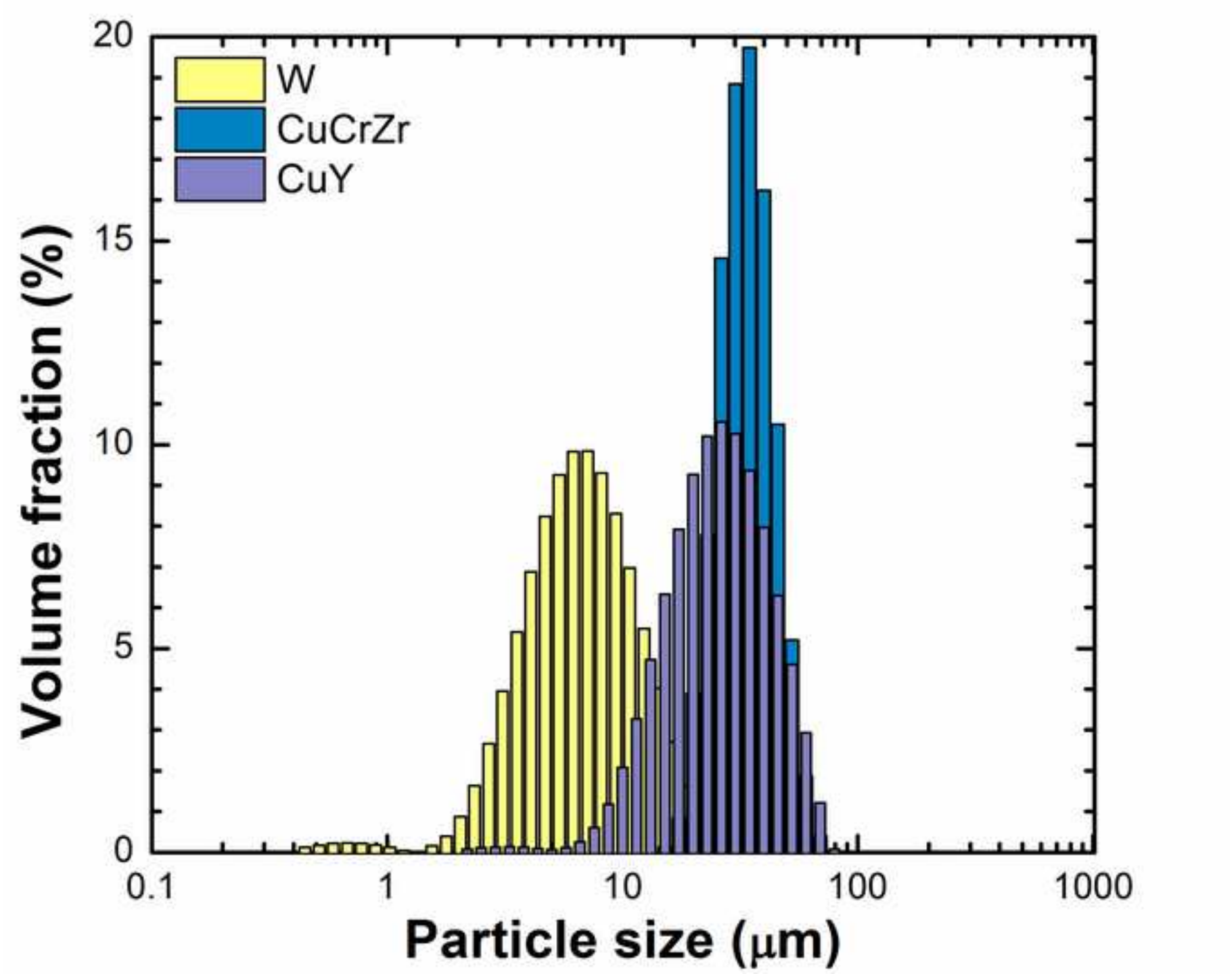

Figure 2

Click here to download high resolution image

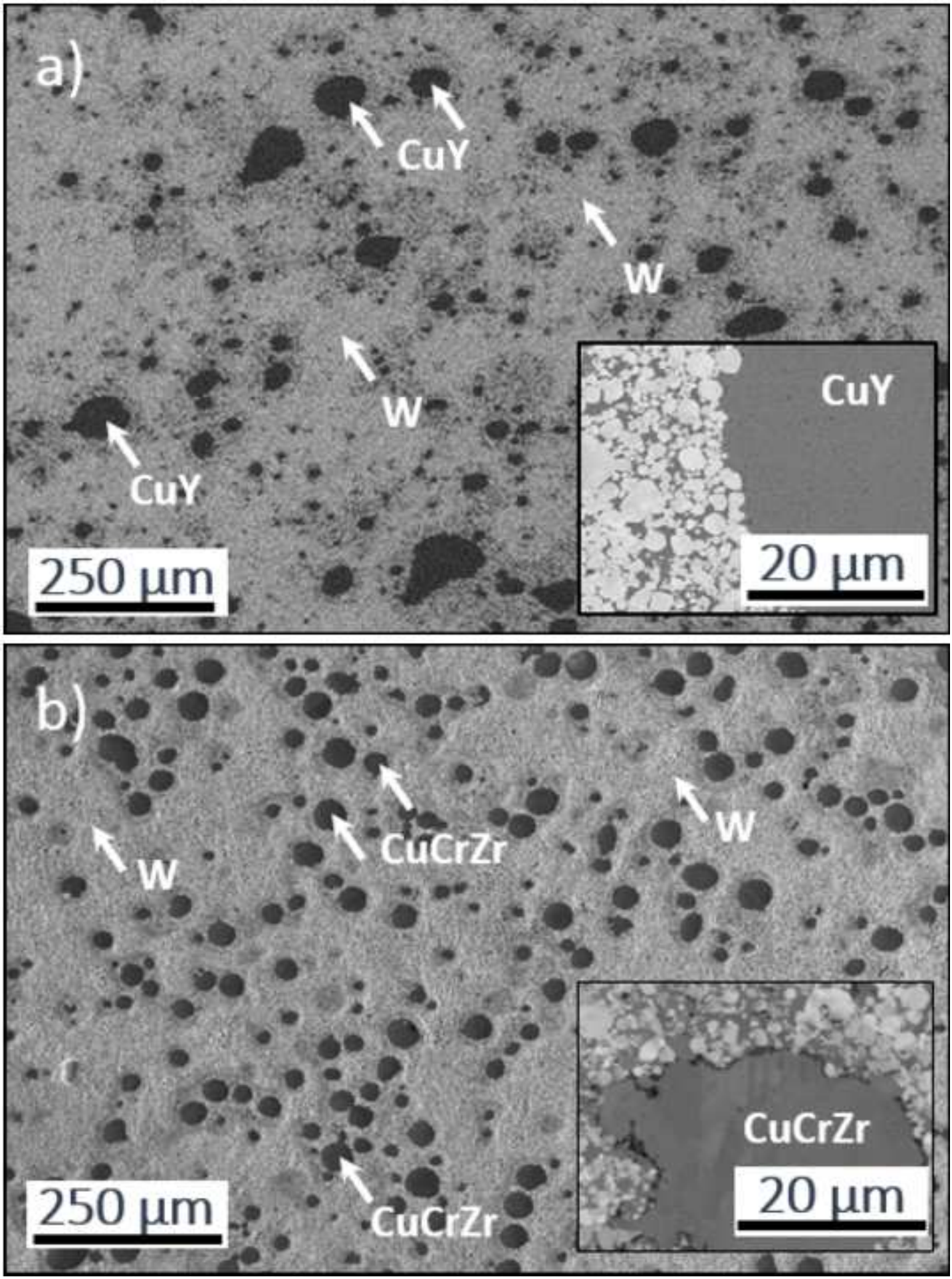

Figure 3
Click here to download high resolution image

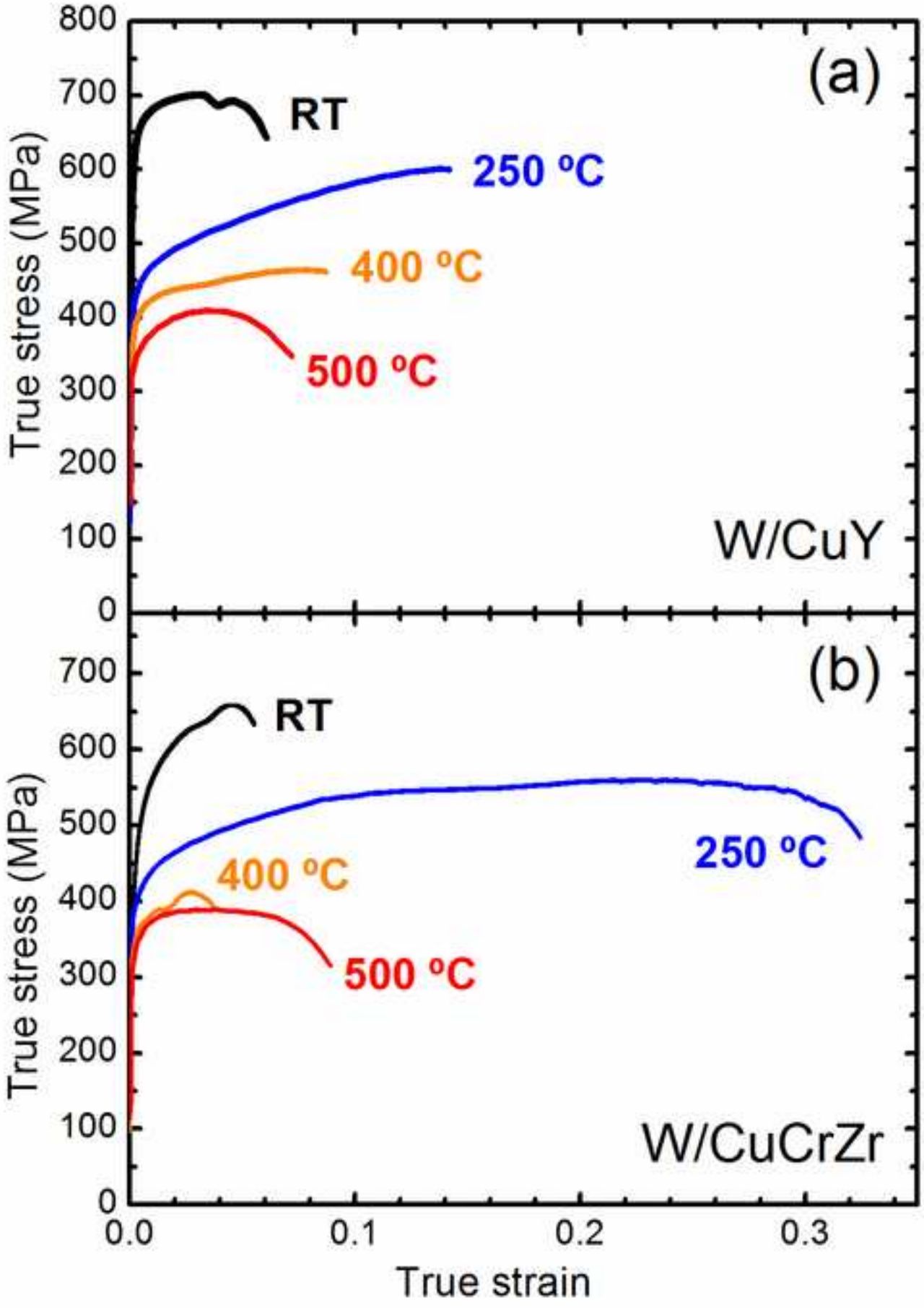

Figure 4
Click here to download high resolution image

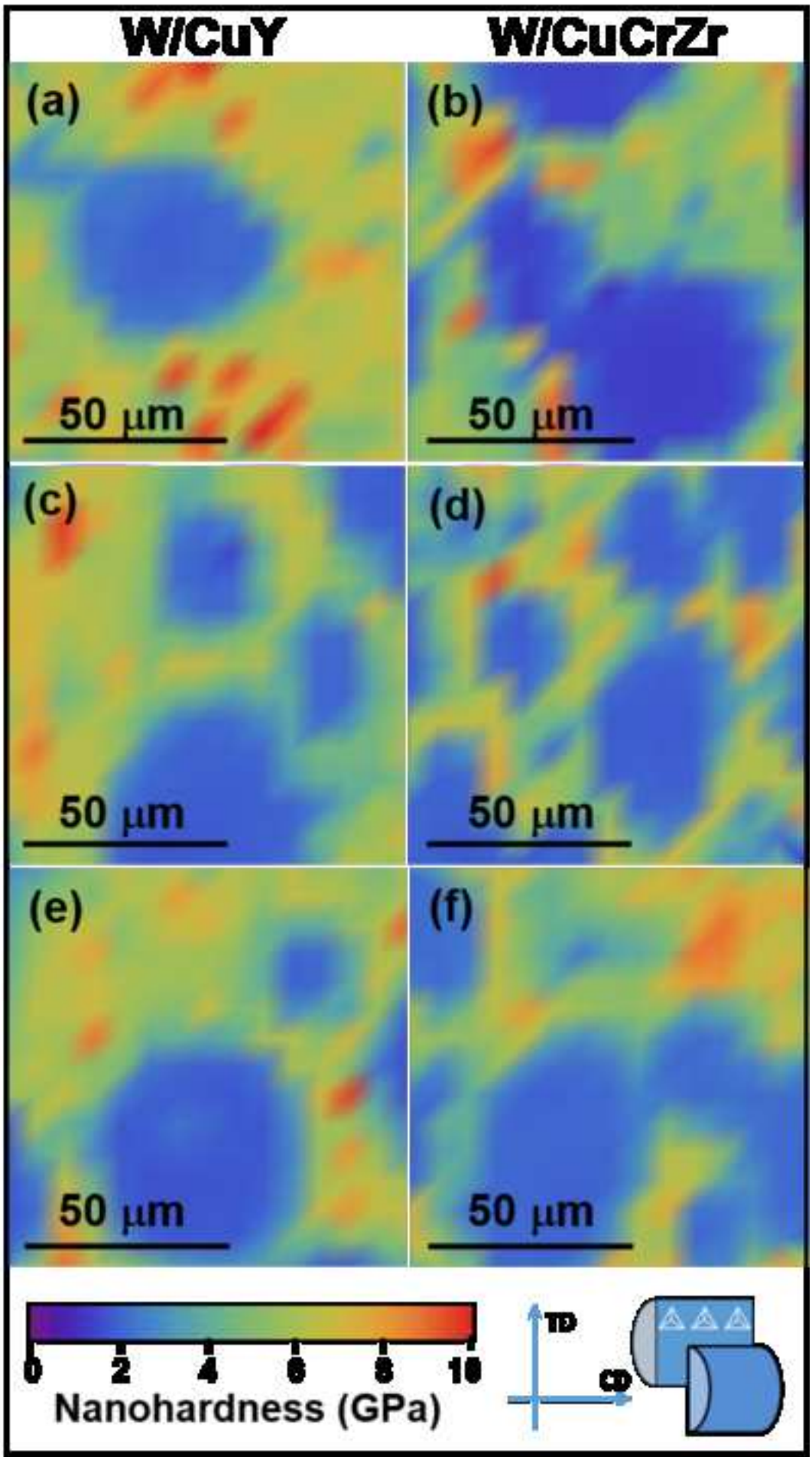

Figure5
Click here to download high resolution image

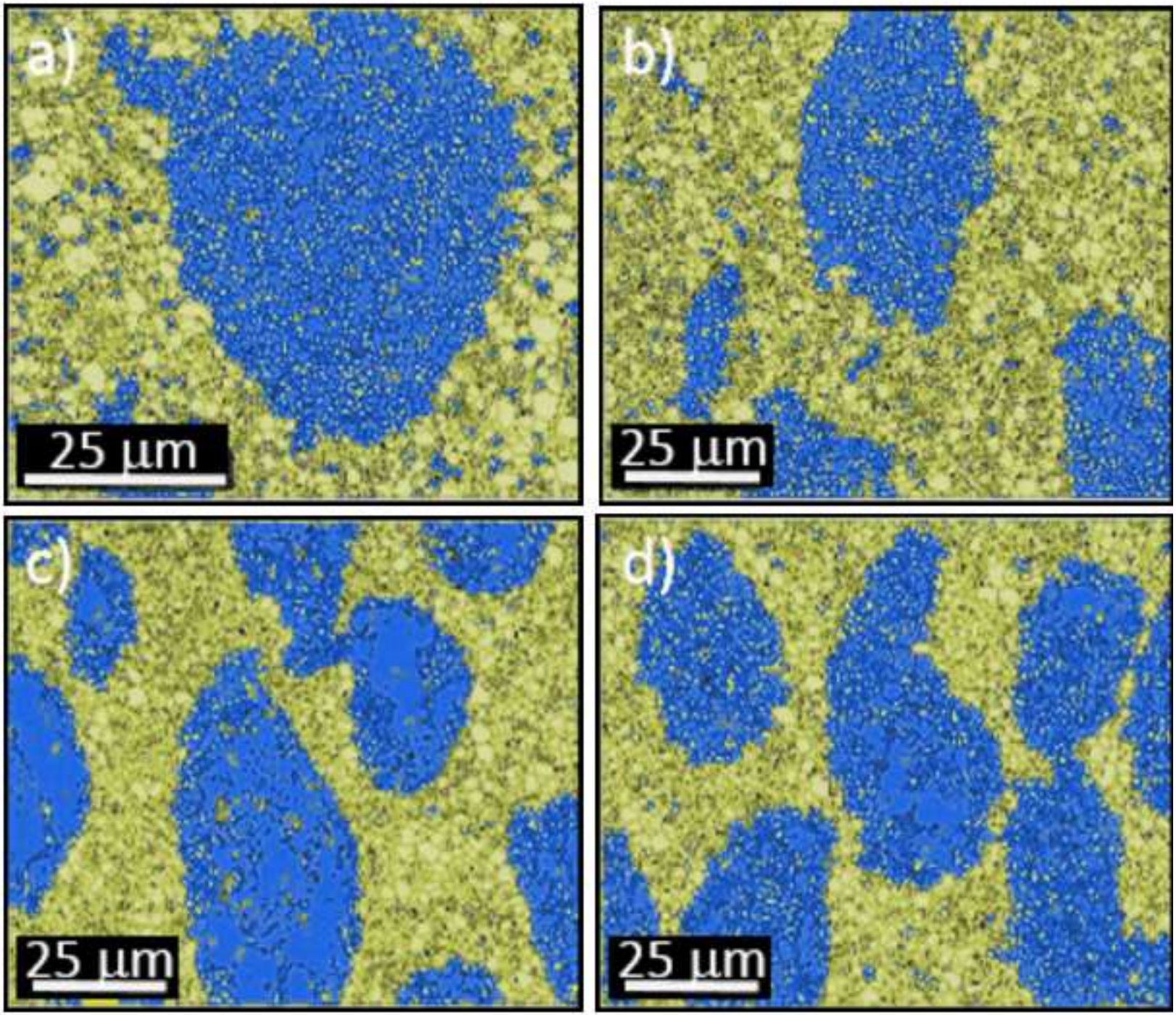

Figure6
Click here to download high resolution image

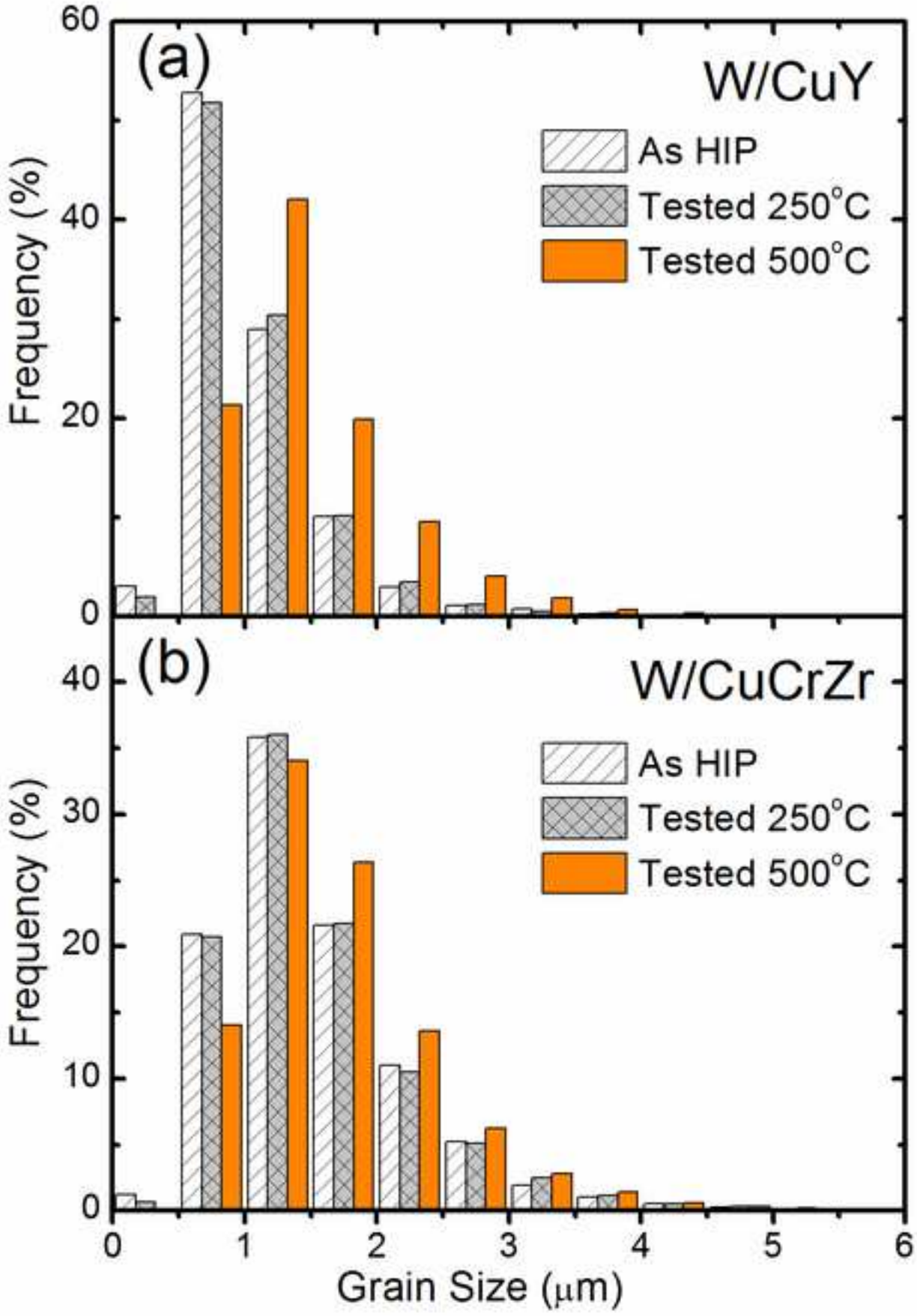

Figure7
Click here to download high resolution image